Letters in Applied NanoBioScience
Open-Access Journal (ISSN: 2284-6808)

Article
Volume 12, Issue 4, 2023, 138
https://doi.org/10.33263/LIANBS124.138

Morphology and Anti-microbial Studies of Zinc Stannate Nanoparticles Constructed *via* Green Synthesis Approach

Yaddanapudi Venkata Bhaskara Lakshmi [1], Peravali Swapna [1,*], Bonige Kishore Babu [1], Yarravarapu Srinivasa Rao [1]

[1] Instrument technology, AU College of Engineering, Visakhapatnam 530003, India; lakshmijeevan2000@gmail.com (V.B.L.Y.); jacobkishore@gmail.com (B.K.B.); srinniwasarau@gmail.com (Y.S.R.);
* Correspondence: Peravali_r2000@yahoo.co.in (P.S.);

Scopus Author ID 9246865000

Received: 15.03.2022; Accepted: 13.04.2022; Published: 8.10.2022

Abstract: In the scientific field, microbial contaminations are growing along with the developments of newer research methodologies. Evaluating anti-microbial activity using newly designed materials has been gaining importance over the years to address this issue. The present work aims to form zinc stannate nanoparticles (ZTO NPs) through bio-synthesis and compare their biological efficiency with the as-synthesized nanoparticles through chemical synthesis. The nanoparticles (Zn_2SnO_4) were synthesized through a hydrothermal method by developing moderate experimental conditions. Three different combinations were synthesized using 2:1 mole ratio of $ZnCl_2$ and $SnCl_2$ precursors, and leaf extracts such as *Aloe barbadensis* mill and *Terminalia catappa* were used in the bio-synthesis method. Sodium hydroxide was used as a mineralizer in the chemical synthesis method. The obtained ZTO NPs were characterized by XRD, SEM-EDS, and UV-Visible spectral techniques. Finally, the antibacterial and anti-fungal activities were evaluated using the Agar-well diffusion method. Competitive biological activity response from the bio-synthesized ZTO NPs against the selected bacterial (*Bacillus subtilis*, *S. Aureus*, *E. Coli*, and *P. Aeruginosa*) and fungal strains (*A. Niger* and C. *albicans*). The synthesized ZTO NPs were highly efficient in exhibiting potential biological activity against the selected microbes.

Keywords: biological activity; bio-synthesis; hydrothermal method; zinc stannate; nanoparticles.

1. Introduction

Zinc stannate is known to act as ternary semiconducting material [1], and about the property, it can exhibit high electron mobility and electrical conductivity and is widely used in piezoelectric nanodevices, photovoltaic devices, polymer-based electronics, etc. [2-5]. They belong to the perovskite group of oxides and are generally crystallized in ilmenite structure enabled by face-centered-cubic (fcc) closed packing [6]. Various synthesis routes such as thermal evaporation [7], co-precipitation [8], low-temperature ion exchange [9], solvothermal [10], high-temperature calcination [11], sol-gel [12], and hydrothermal methods [13-16] were incorporated to form these materials with high purity.

Wang *et al*. [17] have demonstrated the synthesis of zinc stannate nanoparticles (ZTO NPs) in which the morphology was observed to be nanosheets embedded with hollow spheres. The hydrothermal method was used by the research group by including cetyltrimethylammonium bromide (CTAB) as the mineraliser. Geng *et al*. [18] have performed the synthesis of polyhedral ZTO microcrystals by wet chemical methods near 85°C. Zeng *et al*. [19] have reported the formation of ZTO nanocages through zinc acetate and tin (IV) chloride as the precursors *via*. hydrothermal method. The method successfully formed the nanoparticles in the range of 200 – 400 nm scale, which were used in the gas-sensing properties. J. Huang *et al*. [20] have formed porous ZTO nanocubes through zinc sulfate heptahydrate and tin (IV) chloride as the precursors through the thermal treatment method. The NPs obtained in this methodology were observed to be pH sensitive, and the particles were formed in the range of 80 – 100 nm at pH 12.0 and 280 – 310 nm near pH 12.6. The NPs were used in the gas-sensing applications and photocatalytic degradation of Rhodamine B solution (50 mL of 10 mg per L). J. E. Jeronsia *et al*. [21] have reported the antibacterial efficiency of ZTO NPs (Zn_2SnO_4), which were synthesized through the hydrothermal method with chloride salts of zinc and tin as the precursors. The NPs have displayed potential antibacterial activity against gram-positive (*S. Aureus, Bacillus subtilis*) and gram-negative (*K. Pneumonia, E. Coli*) bacteria.

Over the past years, microbial contamination has been identified to be increasing with the growing advancements in scientific research [21, 22, 23]. To inhibit their growth, various materials have been used. Some of these materials are metal oxide nanoparticles like TiO_2, ZnO, Fe_2O_3, WO_3, etc. [24,25]. Nano-metal composites are other biocompatible materials that are efficient in restricting the growth of microorganisms. Composites of TiO_2, such as x % graphene-oxide-TiO_2, were reported to display efficient antibacterial and anti-fungal activities [25]. The materials were able to control the growth of various microorganisms like *Escherichia coli, Staphylococcus aureus, Salmonella paratyphi, Bacillus subtilis* [26,27].

Based on these inputs, it has been observed that there is significant scope for developing biologically active ZTO NPs in a novel approach to obtaining nanoparticles of different morphology. Therefore, the major objective of the present research work is to form ZTO NPs (Zn_2SnO_4) through a bio-synthetic approach by embedding with leaf extracts of *Aloe barbadensis mill* and *Terminalia catappa*. Pure ZTO NPs (without leaf extract) were also synthesized through the hydrothermal method, and all the synthesized NPs were characterized using XRD, SEM-EDS, and UV-Visible spectroscopic techniques. The anti-microbial activity of the synthesized NPs was evaluated against selected bacterial (*Bacillus subtilis, S. aureus, E. coli*, and *P. aeruginosa*) and fungal strains (*A. Niger* and *C. albicans*).

2. Materials and Methods

The chemical reagents used in synthesizing the ZTO NPs and the microorganism strains selected for the anti-microbial studies were discussed under materials and methods. All the experimental results were presented, and these results were compared with the standard literature. The obtained results could be analyzed, and supportive discussions were presented based on the outcomes achieved in the present research work.

Zinc stannate nanoparticles (Zn_2SnO_4, ZTO NPs) were synthesized using Stannous chloride ($SnCl_2$), zinc chloride ($ZnCl_2$), and sodium hydroxide (NaOH), which were procured from Qualigens (AR grade). All the chemical reagents were used in the experimentation without any further purification. The entire process was carried out with double distilled water. To investigate the anti-microbial activity of the synthesized NPs, microorganisms such as gram-positive bacteria (*B. subtilis,* and *S. aureus*), gram-negative bacteria (*P. aeruginosa*, and *E. coli*), and fungal strains such as *A. niger* and *Candida albicans*.

In the present research work, the Zn_2SnO_4 NPs were synthesized using the hydrothermal method [28], and the antibacterial activity of the NPs was evaluated using the Agar-well diffusion method [29].

2.1. Synthesis procedure of ZTO NPs.

2.1.1. Bio-synthesis.

The precursor solution was prepared with 2:1 mole zinc chloride and tin chloride concentrations. In two separate containers, the above solution was added with the leaf extracts of *Aloe barbadensis* mill and *Terminalia catappa*, which acts as mineraliser. These containers were kept under magnetic stirring for about 3 h to perfectly blend the leaf extracts and the chemical precursors. The obtained thick solution was then slowly transferred into a Teflon container equipped with a stainless-steel autoclave. The autoclave is maintained near 200°C for 24 h. The obtained powders were then cleaned and annealed at 600°C for 4 h. Thus, and the obtained materials were ground into fine powders and named ZTO 21A (leaf extract: *Aloe barbadensis mill*) and 21B (leaf extract: *Terminalia catappa*), respectively.

2.1.2. Chemo-synthesis.

A similar procedure was followed for the chemo-synthesis of ZTO NPs, in which sodium hydroxide solution was used as the mineraliser, and it was also able to maintain the pH of the reaction medium. The finally obtained powder was named ZTO 21C.

2.2. Media preparation for evaluating the anti-microbial activity.

In the present research work, Mueller Hinton agar medium was used for regular susceptibility testing of bacteria due to its acceptable reproducibility and satisfactory growth of most pathogens [30]. Sabouraud's dextrose agar was used for the susceptibility testing of fungi [31]. These two media were prepared by dissolving the synthetic powder in distilled water. The medium was adjusted to pH 7.0 with NaOH (1N) and made up to 1 L with remaining distilled water. The conical flask was sealed properly with the help of a cotton plug. The medium and Petri plates (100 mm x 15 mm) were autoclaved at 121°C, 15 lbs for 20 min. The autoclaved medium was allowed to cool to 45°C and transferred into Petri plates (20 ml/plate) under disinfected conditions of laminar airflow.

3. Results and Discussion

3.1. Instrumentation.

The crystalline structure of the ZTO NPs was characterized using X-Ray Diffractometer. Their absorbance was measured using UV-Vis spectra and were recorded using Single Monochromator UV-2600. Field Emission Scanning Electron Microscopy investigated the morphology of the as-synthesized samples.

3.2. Results and discussion.

The results obtained in the characterization of the ZTO NPs and anti-microbial activity studies were presented. All the results were interpreted, and the outcomes were discussed concerning the standard scientific reports.

3.2.1. PXRD analysis.

The crystalline structures of ZTO 21A, 21B, and 21C NPs were identified through the PXRD patterns, and the same were presented in figures 1 to 3, respectively. The diffraction planes (111), (220), (311), (222), (422), and (511) were obtained at 2θ 17.7°, 29.1°, 34.2°, 35.8°, 52.1°, and 54.7° respectively, corresponding to the standard Zn_2SnO_4 material with JCPDS File No. 24-1470 [32]. The average crystallite size (D, nm) was calculated through the FWHM method using Debye-Scherrer's equation.

$$D = \frac{K\lambda}{\beta\ cos\theta}$$

where, λ is the wavelength of the X-ray source used (copper, λ=1.54 A°), β is the line width at the half of maximum intensity, k is Scherer constant, and θ is denoted Braggs angle. This equation obtained the average crystallite size as 17.8, 18.3, and 18.6 nm for ZTO 21A, 21B, and 21C NPs, respectively.

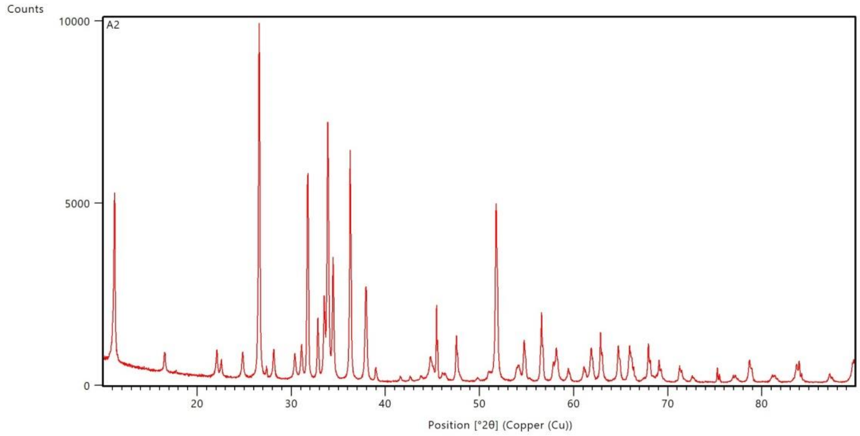

Figure 1. PXRD spectra of ZTO NPs extracted with *Aloe barbadensis mill.*

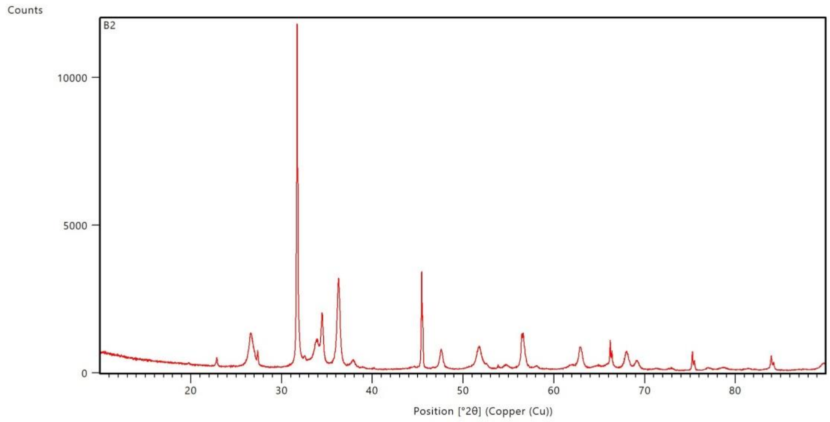

Figure 2. PXRD spectra of ZTO NPs extracted with *Terminalia catappa.*

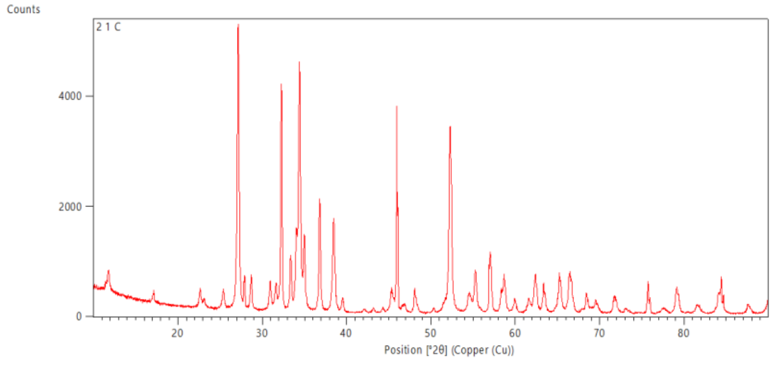

Figure 3. PXRD spectra of ZTO NPs formed through chemo-synthesis.

3.2.2. SEM-EDS.

The SEM images of all the ZTO NPs are shown in figures 4(a), 4(b), and 4(c), respectively. It can be observed that the ZTO NPs formed through the chemo-synthesis method were formed in the form of nano-spheres (figure 4c). Including the leaf extracts in the synthesis method, the ZTO NPs were modified into forming agglomerated spherical-shaped nanoparticles (figures 4a & 4b). Further, the EDS spectra are shown in figures 4(d) and 4(e). In these spectra, the presence of the respective atoms (Zn, Sn, and O) was observed, which confirms the formation of the ZTO NPs.

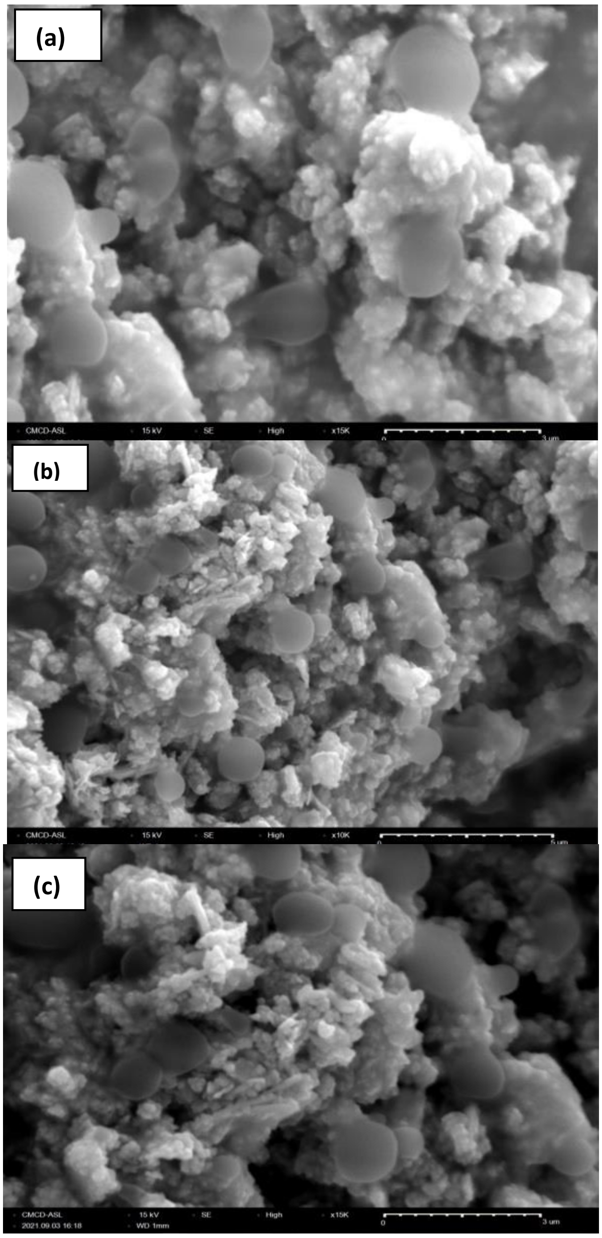

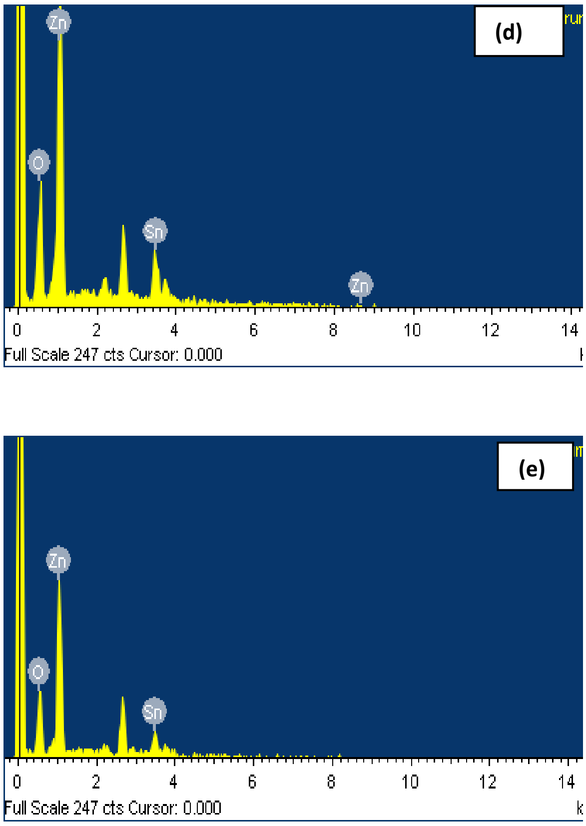

Figure 4. SEM images of (a) ZTO 21A NPs; (b) ZTO 21B NPs; (c) ZTO 21C NPs; EDS spectra of (d) ZTO 21A NPs; (e) ZTO 21B NPs.

3.2.3. UV-Visible spectroscopic studies.

The percentage transmittance (% T) of the synthesized ZTO NPs was measured using a UV-Vis spectrophotometer over the 350 – 1000 nm wavelength range. The % T of ZTO 21A NPs was maximum in 470-500 nm (figure 5). The % T of ZTO 21B NPs has shown a gradual increase in % transmittance with an increase in wavelength and reached a maximum value near 1000 nm (figure 5). The % transmittance of ZTO 21C NPs was maintained in the range of 97

– 98% (figure 5). These results showed that the % transmittance has increased in the ZTO NPs synthesized with the leaf extract of *Terminalia catappa* and *Aloe barbadensis mill* over a broad wavelength range of 380-880 nm, was nearer to that of the ZTO 21C NPs. Hence, there is a subsequent constructive change in the % T of ZTO NPs, including the leaf extracts.

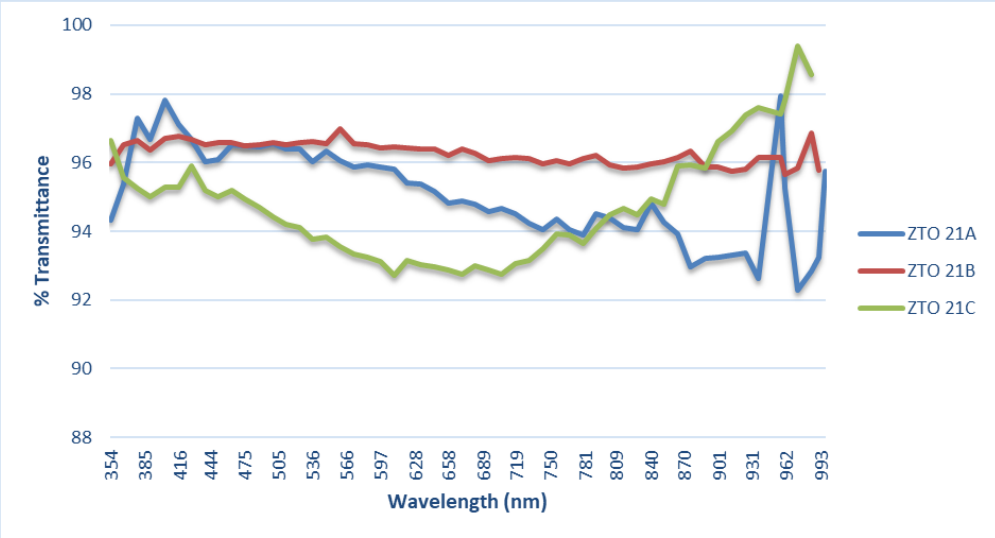

Figure 5. UV-Vis spectra of ZTO 21A, 21B and 21C NPs.

3.2.4. Evaluation of anti-microbial activity (Agar-well diffusion testing).

The cup plate method or agar well diffusion method depends upon the diffusion of antibiotics from a vertical cylinder through a solidified agar layer in a Petri dish or plate to an extent such that the growth of added microorganisms is prevented entirely in a zone around the cylinder containing a solution of the antibiotics.

Antibacterial activities of the compounds investigated were first evaluated by the agar well diffusion method. The standardized cultures of test bacteria were first evenly spread onto the surface of Mueller Hinton Agar plates using sterile cotton swabs, and fungi were spread on Sabouraud's Dextrose Agar plates using sterile cotton swabs. Five wells (6 mm diameter) were made on each plate with a sterile cork borer. Fifty microliters of each compound and positive control were added to wells. Streptomycin (100 μg per mL) was used as the standard drug for comparing the results obtained with the ZTO NPs. Diffusion of compounds, antibiotics, and DMSO was allowed at room temperature for 1 h. All the plates were then covered with lids and incubated at 37^{o}C for 24 h. The quantities of the contents used in the Mueller-Hinton method are shown in Table 1. Post incubation, the plates were measured for the inhibition zone of bacterial growth. The anti-microbial activity of the compounds was expressed in terms of the average diameter of the inhibition zone (in mm). Compounds with an inhibition zone diameter of less than 6 mm are inactive.

Table 1. Composition of Mueller Hinton Agar.

S. No.	Name of the ingredient	Quantity (g)
1	Beef Infusion	3.00
2	Casein acid hydrolysate	17.50
3	Starch	1.50
4	Agar	17.50
5	Final pH (at 25°C)	7.3 + 0.2

The anti-microbial activity studies were conducted with ZTO NPs obtained at 5000 rpm; it was observed that the inhibition tendency was predominant at higher concentrations of the medium. The ZOI for all the selected bacterial strains was higher for ZTO 21B NPs than

21C and 21A NPs, at 10 mg per L concentration. The ZTO 21B NPs have shown maximum ZOI with all the selected bacterial strains, and the ZTO 21C NPs have exhibited the next superior activity after 21B NPs. However, at 5 mg per L concentration of the NPs, the activity was almost negligible against *S. aureus* and *E. Coli* strains. The bacterial strains were significantly inhibited at higher concentrations (10 mg per L). Moreover, the antibacterial activity of the ZTO 21A NPs was predominantly more than ZTO 21C NPs. These results indicate the effectiveness of the green synthesized ZTO NPs in inhibiting the growth of the selected bacterial strains, and the results are presented in Table 2.

In the anti-fungal activity studies, the ZOI of *A.niger* was highest with ZTO 21B NPs. The ZTO 21A & 21C NPs have shown equal performance against the fungal strain at both concentrations. The ZOI of the fungal strain *C. albicans* was observed to be maximum with ZTO 21A NPs than the 21C NPs. These results indicate the ability of the green synthesized ZTO NPs to perform efficient anti-fungal activity. The results are presented in Table 3, and the images of anti-microbial studies are shown in figure 6.

Table 2. Zone of inhibition antibacterial activity of compounds

S. No	**ZTO NPs**	**Zone of inhibition (mm)**							
		Bacillus subtilis		***S. aureus***		***E. coli***		***P. aeruginosa***	
		10mg	5mg	10mg	5mg	10mg	5mg	10mg	5mg
1	21A	10	8	12	10	10	8	12	8
2	21B	21	17	16	14	18	14	13	8
3	21C	16	8	8	0	10	0	10	7

Table 3. Zone of inhibition anti-fungal activity of compounds.

S. No	ZTO NPs	Zone of inhibition (mm)			
		A. niger		*C. albicans*	
		10mg	5mg	10mg	5mg
1	21A	8	0	14	12
2	21B	12	8	16	13
3	21C	8	0	8	0

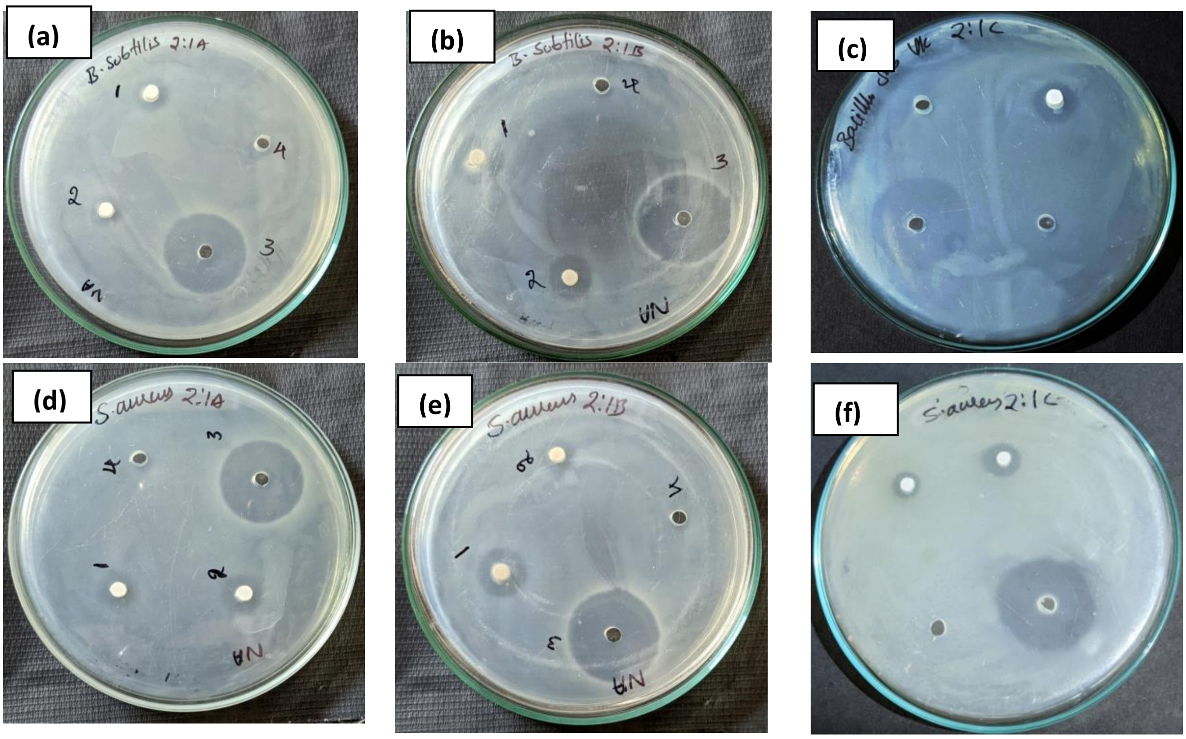

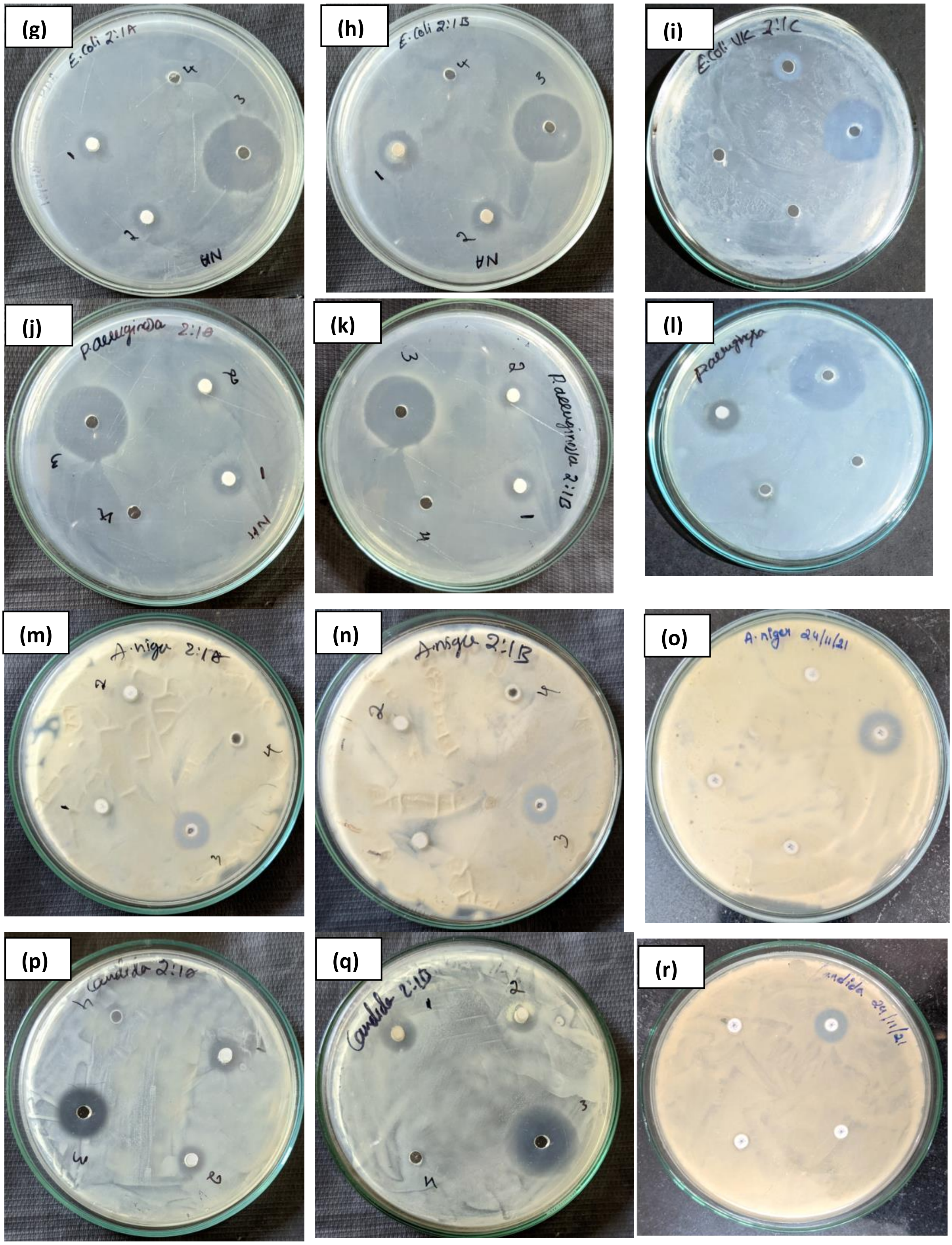

Figure 6. (a) anti-bacterial activity of ZTO 21A NPs against *B. Subtilis* (1) 10 mg; (2) 5 mg; (3) Streptomycin 100 µg; (4) Negative control (DMSO). (b) activity of ZTO 21B NPs& (c) ZTO 21C NPs. (d) anti-bacterial activity of ZTO 21A NPs against *S.aureus* (1) 10 mg; (2) 5 mg; (3) Streptomycin 100 µg; (4) Negative control (DMSO). (e) activity of ZTO 21B NPs & (f) ZTO 21C NPs. (g) anti-bacterial activity of ZTO 21A NPs against *E. Coli* (1) 10 mg; (2) 5 mg; (3) Streptomycin 100 µg; (4) Negative control (DMSO). (h) activity of ZTO 21B NPs & (i) ZTO 21C NPs. (j) anti-bacterial activity of ZTO 21A NPs against *P. aeruginosa* (1) 10 mg; (2) 5 mg; (3) Streptomycin 100 µg; (4) Negative control (DMSO).(k) activity of ZTO 21B NPs & (l) ZTO 21C NPs. (m) anti-fungal activity of ZTO 21A NPs against *A. niger* (1) 10 mg; (2) 5 mg; (3) Streptomycin 100 µg; (4) Negative control (DMSO). (n) activity of ZTO 21B NPs & (o) ZTO 21C NPs. (p) anti-fungal activity of ZTO 21A NPs against *C. albicans* (1) 10 mg; (2) 5 mg; (3) Streptomycin 100 µg; (4) Negative control (DMSO). (q) activity of ZTO 21B NPs & (r) ZTO 21C NPs.

After analyzing various research articles, it was found that the nanoparticles constructed through the leaf extracts can exhibit various biological functions. Further, the eco-friendly synthesis of nanoparticles has been challenging the traditional chemo-synthesis of nanoparticles in displaying equal and, in some cases, potential biological, photocatalytic, and photovoltaic applications. In the present research scenario, finding an environmentally benign methodology to address the existing research limitations has become inevitable. The present work contributes to this research loop as well. The research article presents the anti-microbial activity studies of zinc stannate nanoparticles synthesized through the leaf extracts of *Aloe barbadensis mill* and *Terminalia catappa*. The XRD plots have revealed the formation of corresponding diffraction planes of the ZTO NPs, and the average crystallite size of the NPs was observed to form in the range of 14-18 nm. The morphology of the NPs through these leaf extracts has changed from nanoplates to nano-spherical particles. Further, the transmittance of the NPs formed through bio-synthesis was slightly higher than those formed through chemo-synthesis. The biological activity of the ZTO NPs was investigated against various bacterial and fungal strains. In this regard, the biological activity of some of the potential nanoparticles synthesized through the leaf extracts of *Aloe barbadensis mill* and *Terminalia catappa*.Rajkumari *et al*. [33] have demonstrated the antibacterial activity of titanium dioxide nanoparticles extracted with *Aloe barbadensis mill* against *P. aeruginosa*. The aqueous leaf extract acted as a reducing and stabilizing agent inducing the highest cell viability in 30.76±3.96%. This profound activity was observed with 31.25 µg per mL of the NPs. Bhuvan Ran *et al.* [34] have presented the biological activity of eco-friendly synthesized CeO_2 NPs using *Aloe barbadensis mill* extract. The average crystallite size of these NPs was found to be 13 nm, and the antibacterial activity was investigated against *Escherichia coli*, *Klebsiella pneumoniae, Pseudomonas aeruginosa,* and anti-fungal activity was performed against Aflatoxigenic *Aspergillus flavus* PPBS1. Highest zone of inhibition was observed with *P. aeruginosa*in on the order of 10±1 mm. As a whole, the maximum growth inhibition was noticed to be 3 cm, and % of inhibition was obtained as 75% at a concentration of 5µg per mL. Vijaykumar *et al*. [35] have synthesized ZnO NPs through the leaf extract of *Aloe barbadensis mill*. The NPs were obtained in a hexagonal wurtzite structure with an average crystallite size of 16 nm. The NPs were applied in biosensing and photocatalytic activity studies. Naresh Kumar *et al*. [36] have reported the fabrication of ZnO nanoparticles extracted with the fruit pigments of *Terminalia catappa*. The research has exposed the fruit extract's effectiveness in generating potential dye-sensitized photovoltaic cells, with 1.58% efficiency. Balaprasad [37] has performed the eco-friendly synthesis of gold nanoparticles through the leaf extract of *Terminalia catappa (Almond)*. The leaf extract was observed to act as a reducing and stabilizing agent in forming the nanoparticles with high purity. The absorbance of the Au-NPs formed through the leaf extract was higher than the absorbance of the pure leaf extract. The average crystallite size of the NPs was formed in the range of 20-25 nm scale, and the established method successfully formed a green synthesis technique. Lembang *et al*. [38] have presented their research article on the green synthesis of Nd_2O_3 NPs through aqueous leaf extract of *Terminalia catappa*. The absorbance of the NPs was higher than that of the leaf extract, and the average crystallite size was observed to be less than 100 nm. In general, the anti-microbial activity of the NPs depends on their composition, particle size, and morphology [39]. In a typical anti-microbial mechanism, the microbes and the NPs will be associated through electrostatic attraction, which disrupts the cell walls of the microbes. This phenomenon leads to the permanent disability of the selected microbial strains [40-45]. In the present studies, all the synthesized ZTO NPs (21A & 21B) exhibited antibacterial and anti-fungal activities. The NPs formed through the bio-synthesis method have shown competitive biological activity compared to those formed through chemo-synthesis. This phenomenon was observed in the zone of inhibitions of the bacterial strains *Bacillus subtilis*, *S. Aureus*, *P. Aeruginosa*, and the fungal strain *C. albicans*.

These outcomes propagate that the synthesized ZTO NPs are biologically active, which drives them toward exhibiting potential biomedical and pharmaceutical applications. Further, it was also presented in the scientific literature that the ZTO NPs are applied in photovoltaic devices owing to their higher conducting properties. In these aspects, the synthesized ZTO NPs can display conducting properties by coating with a suitable metal halide salt such as magnesium fluoride (MgF_2). These MgF_2-coated ZTO NPs can also demonstrate higher transmittance, and that would enhance the conducting properties of the synthesized zinc stannate nanoparticles. These aspects can contribute to the future scope of the present research work.

4. Conclusions

Zinc stannate nanoparticles with composition Zn_2SnO_4 were synthesized using reducing/stabilizing agents such as the leaf extracts of *Aloe barbadensis mill* and *Terminalia catappa*. Chemical synthesis was also conducted with sodium hydroxide as the mineralizer. The crystalline nature and the morphology of the NPs were interpreted through XRD and SEM-EDS instrumental techniques. The transmittance of the NPs was measured through a UV-Vis spectrophotometer, and all the characterization results have shown the significance of forming the NPs through the leaf extracts. The anti-microbial activity of the NPs was investigated against selected bacterial and fungal strains. In these studies, the ZTO NPs extracted with *Terminalia catappa* have presented higher biological performance. Further, the ZTO NPs extracted with *Aloe barbadensis mill* have displayed reasonable activity compared to those synthesized through a pure chemical pathway. Hence, it was concluded that the ZTO NPs are highly efficient in inhibiting the growth of various microbes. The established methodology was successful in all aspects of scientific research.

Funding

This research received no external funding.

Acknowledgments

The authors thank the Inorganic chemistry laboratory, Andhra University (Visakhapatnam, India), for providing the synthesis facilities and the nanotechnology lab for characterization results.

Conflicts of Interest

The authors declare no conflict of interest.

References

1. An, S.; Jin, Ch.; Kim, H.; Lee, S.; Jeong, B.; Lee, C. Synthesis, structure and luminescence properties of $ZnSnO_3$ nanowires. *NANO: Brief Reports and Reviews* **2012**, *7*, 1-7, https://doi.org/10.1142/S1793292012500130.

2. Stambolova, I.; Konstantinov, K.; Kovacheva, D.; Peshev, P.; Donchev, T. Spray Pyrolysis Preparation and Humidity Sensing Characteristics of Spinel Zinc Stannate Thin Films. *Journal of Solid State Chemistry* **1997**, *128*, 305-309, https://doi.org/10.1006/jssc.1996.7174.
3. Nikolić, N.; Srećković, T.; Ristić, M.M. The influence of mechanical activation on zinc stannate spinel formation. *Journal of the European Ceramic Society* **2001**, *21*, 2071-2074, https://doi.org/10.1016/S0955-2219(01)00174-1.
4. Coutts, T.J.; Young, D.L.; Li, X.; Mulligan, W.P.; Wu, X. Search for improved transparent conducting oxides: A fundamental investigation of CdO, Cd2SnO4, and Zn2SnO4. *Journal of Vacuum Science & Technology A* **2000**, *18*, 2646-2660, https://doi.org/10.1116/1.1290371.
5. Naqeeb, A.; Haq, E.S.R.; Imran Shahzad, M.; Shahzad, N.; Rehman, W.; Waseem, M.; Ahmad, P.; Khalilov, U. Ficus carica mediated synthesis of simulated solar light driven nano-sized zinc stannate photocatalyst for the degradation of methylene blue. *Research square* **2021**, *4*, 1-15, https://doi.org/10.21203/rs.3.rs-435724/v1.
6. Geng, B.; Fang, C.; Zhan, F.; Yu, N. Synthesis of Polyhedral ZnSnO3 Microcrystals with Controlled Exposed Facets and Their Selective Gas-Sensing Properties. *Small* **2008**, *4*, 1337-1343, https://doi.org/10.1002/smll.200701177.
7. Zhang, T.; Shen, Y.; Zhang, R. Ilmenite structure-type β-CdSnO3 used as an ethanol sensing material. *Materials Letters* **1995**, *23*, 69-71, https://doi.org/10.1016/0167-577X(95)00007-0. (b) Xu, J.; Jia, X.; Lou, X.; Xi, G.; Han, J.; Gao, Q. Selective detection of HCHO gas using mixed oxides of ZnO/ZnSnO3. *Sensors and Actuators B: Chemical* **2007**, *120*, 694-699, https://doi.org/10.1016/j.snb.2006.03.033.
8. Patiño-Ruiz, D.A.; Meramo-Hurtado, S.I.; González-Delgado, Á.D.; Herrera, A. Environmental Sustainability Evaluation of Iron Oxide Nanoparticles Synthesized via Green Synthesis and the Coprecipitation Method: A Comparative Life Cycle Assessment Study. *ACS Omega* **2021**, *6*, 12410-12423, https://doi.org/10.1021/acsomega.0c05246.
9. Xue, X.Y.; Chen, Y.J.; Liu, Y.G.; Shi, S.L.; Wang, Y.G.; Wang, T.H. Synthesis and ethanol sensing properties of indium-doped tin oxide nanowires. *Applied Physics Letters* **2006**, *88*, https://doi.org/10.1063/1.2203941.
10. Wang, S.; Zhao, L.; Huang, W.; Zhao, H.; Chen, J.; Cai, Q.; Jiang, X.; Lu, C.; Shi, W. Solvothermal synthesis of CoO/BiVO4 p-n heterojunction with micro-nano spherical structure for enhanced visible light photocatalytic activity towards degradation of tetracycline. *Materials Research Bulletin* **2021**, *135*, https://doi.org/10.1016/j.materresbull.2020.111161.
11. Shi, J.-B.; Wu, P.-F.; Lin, H.-S.; Lin, Y.-T.; Lee, H.-W.; Kao, C.-T.; Liao, W.-H.; Young, S.-L. Synthesis and characterization of single-crystalline zinc tin oxide nanowires. *Nanoscale Res Lett* **2014**, *9*, https://doi.org/10.1186/1556-276X-9-210.
12. Zhao, Y.; Hu, L.; Liu, H.; Liao, M.; Fang, X.; Wu, L. Band Gap Tunable Zn2SnO4 Nanocubes through Thermal Effect and Their Outstanding Ultraviolet Light Photoresponse. *Scientific Reports* **2014**, *4*, https://doi.org/10.1038/srep06847.
13. Akhtar, A.; Chu, X.; Liang, S.; Dong, Y.; He, L.; Zhang, K. Enhanced formaldehyde sensing properties of MoS2-Zn2SnO4 nanocomposites synthesized via hydrothermal method. *Inorganic Chemistry Communications* **2021**, *127*, https://doi.org/10.1016/j.inoche.2021.108503.
14. Palpandi, K.; Raman, N. Hydrothermally synthesized a pyrochlore-type bismuth stannate (Bi2Sn2O7): Efficient electrochemical detection of nitroxoline. *Journal of Electroanalytical Chemistry* **2021**, *899*, https://doi.org/10.1016/j.jelechem.2021.115679.
15. Li, X.; Zhang, N.; Liu, C.; Adimi, S.; Zhou, J.; Liu, D.; Ruan, S. Enhanced gas sensing properties for formaldehyde based on ZnO/Zn2SnO4 composites from one-step hydrothermal synthesis. *Journal of Alloys and Compounds* **2021**, *850*, https://doi.org/10.1016/j.jallcom.2020.156606.
16. Ben Ali, M.; Nasser, R.; Alshahrani, S.M.; Al-Shamiri, H.A.S.; Elgammal, B.; Elhouichet, H. Synthesis, characterization, and visible-light photocatalytic activity of transition metals doped ZTO nanoparticles. *Ceramics International* **2021**, *47*, 32882-32890, https://doi.org/10.1016/j.ceramint.2021.08.185.
17. Foletto, E.L.; Simões, J.M.; Mazutti, M.A.; Jahn, S.L.; Muller, E.I.; Pereira, L.S.F.; Flores, E.M.d.M. Application of Zn2SnO4 photocatalyst prepared by microwave-assisted hydrothermal route in the degradation of organic pollutant under sunlight. *Ceramics International* **2013**, *39*, 4569-4574, https://doi.org/10.1016/j.ceramint.2012.11.053.
18. Chen, Z.; Cao, M.; Hu, C. Novel Zn2SnO4 Hierarchical Nanostructures and Their Gas Sensing Properties toward Ethanol. *The Journal of Physical Chemistry C* **2011**, *115*, 5522-5529, https://doi.org/10.1021/jp111785t.
19. Šepelák, V.; Becker, S.M.; Bergmann, I.; Indris, S.; Scheuermann, M.; Feldhoff, A.; Kübel, C.; Bruns, M.; Stürzl, N.; Ulrich, A.S.; Ghafari, M.; Hahn, H.; Grey, C.P.; Becker, K.D.; Heitjans, P. Nonequilibrium structure of Zn2SnO4 spinel nanoparticles. *Journal of Materials Chemistry* **2012**, *22*, 3117-3126, https://doi.org/10.1039/C2JM15427G.
20. Wang, W.W.; Zhu, Y.J.; Yang, L.X. ZnO–SnO2 Hollow Spheres and Hierarchical Nanosheets: Hydrothermal Preparation, Formation Mechanism, and Photocatalytic Properties. *Advanced functional materials* **2007**, *17*, 59-64, https://doi.org/10.1002/adfm.200600431.

21. Miyauchi, M.; Liu, Z.; Zhao, Z.-G.; Anandan, S.; Hara, K. Single crystalline zinc stannate nanoparticles for efficient photo-electrochemical devices. *Chemical Communications* **2010**, *46*, 1529-1531, https://doi.org/10.1039/B921010E.
22. Zeng, Y.; Zhang, T.; Fan, H.; Fu, W.; Lu, G.; Sui, Y.; Yang, H. One-Pot Synthesis and Gas-Sensing Properties of Hierarchical ZnSnO3 Nanocages. *The Journal of Physical Chemistry C* **2009**, *113*, 19000-19004, https://doi.org/10.1021/jp905230h.
23. Huang, J.; Xu, X.; Gu, C.; Wang, W.; Geng, B.; Sun, Y.; Liu, J. Size-controlled synthesis of porous ZnSnO3 cubes and their gas-sensing and photocatalysis properties. *Sensors and Actuators B: Chemical* **2012**, *171-172*, 572-579, https://doi.org/10.1016/j.snb.2012.05.036.
24. Wang, F.; Shi, Z.; Gong, F.; Jiu, J.; Adachi, M. Morphology Control of Anatase TiO2 by Surfactant-assisted Hydrothermal Method* *Supported by the Natural Science Foundation of Tianjin (No.06YFJMJC05000). *Chinese Journal of Chemical Engineering* **2007**, *15*, 754-759, https://doi.org/10.1016/S1004-9541(07)60158-X.
25. Zhou, Y.S.; Jiang, WG. Study on properties of composite oxides TiO_2/SiO_2. *Chin. J. Chem. Eng.* **2002**, *10*, 349-353.
26. Sekhar, R.S.; Douglas, S.P. Evaluation of Anti-microbial activity of graphene oxide-TiO_2 nanocomposites with variable compositions. *Res. J. Chem. and Env.* **2021**, *10*, 80-83, https://doi.org/10.25303/2510rjce8083.
27. Choi, S.-H.; Hwang, D.; Kim, D.-Y.; Kervella, Y.; Maldivi, P.; Jang, S.-Y.; Demadrille, R.; Kim, I.-D. Amorphous Zinc Stannate (Zn2SnO4) Nanofibers Networks as Photoelectrodes for Organic Dye-Sensitized Solar Cells. *Advanced functional materials* **2013**, *23*, 3146-3155, https://doi.org/10.1002/adfm.201203278.
28. Sekhar, R.S.; Douglas, S.P. Evaluation of anti-microbial activity of x% graphene oxide-titania nanocomposites. *Res. J. Chem. and Environ.* **2021**, *10*, 80-83.
29. Koneru, B.; Shi, Y.; Wang, Y.-C.; Chavala, S.H.; Miller, M.L.; Holbert, B.; Conson, M.; Ni, A.; Di Pasqua, A.J. Tetracycline-Containing MCM-41 Mesoporous Silica Nanoparticles for the Treatment of Escherichia coli. *Molecules* **2015**, *20*, 19690–19698, https://doi.org/10.3390/molecules201119650.
30. Nurjadi, D.; Chanthalangsy, Q.; Zizmann, E.; Stuermer, V.; Moll, M.; Klein, S.; Boutin, S.; Heeg, K.; Zanger, P.; Zhang, K. Phenotypic Detection of Hemin-Inducible Trimethoprim-Sulfamethoxazole Heteroresistance in Staphylococcus aureus. *Microbiology Spectrum* **2021**, *9*, e01510-21, https://doi.org/10.1128/Spectrum.01510-21.
31. Geethalakshmi, V.; Jasmine, K.A.; John, P.A.; Priya, P. Effectiveness of Sabouraud's Dextrose Agar and Dermatophyte Test Medium in Detection of Candidiasis and Dermatophytosis in Superficial Skin Lesion. *Journal of Clinical & Diagnostic Research* **2021**, *15*, 11-15.
32. Stoimenov, P.K.; Klinger, R.L.; Marchin, G.L.; Klabunde, K.J. Metal Oxide Nanoparticles as Bactericidal Agents. *Langmuir* **2002**, *18*, 6679-6686, https://doi.org/10.1021/la0202374.
33. Fernández-Mazarrasa, C.; Mazarrasa, O.; Calvo, J.; del Arco, A.; Martínez-Martínez, L. High Concentrations of Manganese in Mueller-Hinton Agar Increase MICs of Tigecycline Determined by Etest. *Journal of Clinical Microbiology* **2009**, *47*, 827-829, https://doi.org/10.1128/JCM.02464-08.
34. Akgül, Ö.; Çerikçioğlu, N. Hypertonic Sabouraud Dextrose Agar as a Substrate for Differentiation of Candida dubliniensis. *Mycopathologia* **2009**, *167*, https://doi.org/10.1007/s11046-009-9187-7.
35. Ayesha, B.; Jabeen, U.; Naeem, A.; Kasi, P.; Malghani, M.N.K.; Khan, S.U.; Akhtar, J.; Aamir, M. Synthesis of zinc stannate nanoparticles by sol-gel method for photocatalysis of commercial dyes. *Results in Chemistry* **2020**, *2*, https://doi.org/10.1016/j.rechem.2020.100023.
36. Rajkumari, J.; Magdalane, C.M.; Siddhardha, B.; Madhavan, J.; Ramalingam, G.; Al-Dhabi, N.A.; Arasu, M.V.; Ghilan, A.K.M.; Duraipandiayan, V.; Kaviyarasu, K. Synthesis of titanium oxide nanoparticles using *Aloe barbadensis* mill and evaluation of its antibiofilm potential against Pseudomonas aeruginosa PAO1. *Journal of Photochemistry and Photobiology B: Biology* **2019**, *201*, https://doi.org/10.1016/j.jphotobiol.2019.111667.
37. Bhuvan Raj, N.; Pavithra Gowda, N.T.; Pooja, O.S.; Sukrutha, S.K.; Purushotham, B.; Nagaswarupa, H.P.; Anil Kumar, M.R.; Surendra, B.S.; Shekhar, T.R.S.; Prashantha, S.C.; Eco-friendly synthesis of CeO_2 NPs using *Aloe barbadensis Mill* extract: Its biological and photocatalytic activities for industrial dye treatment applications. *J. Photochem. and Photobio.* **2021**, *7*, https://doi.org/10.1016/j.jpap.2021.100038.
38. Vijayakumar, D.J.; Patil, K.M.; Chougala, S.L.; Inamdar, R.S.; Goudar, M.K.; Biogenic Synthesis and Characterization of ZnO Nanoparticles from *Aloe barbadensis Miller* Leaf Extract, *Macromoleccular symposia*, **2021**, 400 (1), 2100177. https://doi.org/10.1002/masy.202100177.
39. Kumar, P.N.; Sakthivel, K.; Saravanakumar, M.; Yuvapragasam, A.; Vijayakumar, B. *Terminalia catappa* Fruit Pigments for Dye Sensitized Solar Cell Applications. *To Chemistry Journal* **2018**, *1*, 50-56.
40. Balaprasad, A.; Biosynthesis of Gold Nanoparticles (Green-Gold) Using Leaf Extract of *Terminalia catappa*. *E-J. Chem.* **2010**, *7*, 1334-1339, https://doi.org/10.1155/2010/745120.
41. Lembang, M.S; Yulizar, Y.; Sudirman, S.; Apriandanu, D.O.B. A Facile Method for Green Synthesis of Nd_2O_3 Nanoparticles Using Aqueous Extract of *Terminalia catappa* Leaf. *AIP Conference Proceedings 2023* **2018**, https://doi.org/10.1063/1.5064090.
42. Musee, N.; Thwala, M.; Nota, N. The antibacterial effects of engineered nanomaterials: implications for wastewater treatment plants. *J. Environ. Monit.* **2011**, *13*, 1164-1183, https://doi.org/10.1039/C1EM10023H.

43. Applerot, G.; Lellouche, J.; Perkas, N.; Nitzan, Y.; Gedanken, A.; Banin, E. ZnO nanoparticle-coated surfaces inhibit bacterial biofilm formation and increase antibiotic susceptibility. *RSC Advances* **2012**, *2*, 2314-2321, https://doi.org/10.1039/C2RA00602B.
44. Iqbal, F.; Ahmed, A. Antibacterial activity of *Aloe barbadensis Mill*. *Polish Journal of Environmental Studies* **2021**, *30*, 3637-3643, https://doi.org/10.15244/pjoes/130041.
45. Hevira, L.; Zilfa; Rahmayeni; Ighalo, J.O.; Aziz, H.; Zein, R. *Terminalia catappa* shell as low-cost biosorbent for the removal of methylene blue from aqueous solutions. *Journal of Industrial and Engineering Chemistry* **2021**, *97*, 188-199, https://doi.org/10.1016/j.jiec.2021.01.028.